



Wiley Analytical Science

Virtual Conference

The 5th edition of the Wiley Analytical Science Conference starts November 8, 2022!

Featured Sessions:

- **Integration of X-ray microscopy and finite elements into a digital twin**

Thurs Nov 10, 10:00 - 10:30 AM EST / 4:00 - 4:30 PM CET

- **Optimization of Cryo TEM lamella preparation workflows to be faster and more accessible**

Wed Nov 16, 10:00 - 11:00 AM EST / 4:00 - 5:00 PM CET

events.bizzabo.com/WASconferenceFall2022



Seeing beyond



WILEY

Self-Powered, Implantable, and Wirelessly Controlled NO Generation System for Intracranial Neuroglioma Therapy

Shuncheng Yao, Minjia Zheng, Zhuo Wang, Yunchao Zhao, Shaobo Wang, Zhirong Liu, Zhou Li, Yunqian Guan,* Zhong Lin Wang,* and Linlin Li*

Gas therapy is an emerging technology for improving cancer therapy with high efficiency and low side effects. However, due to the existence of the gatekeeper of the blood–brain barrier (BBB) and the limited availability of current drug delivery systems, there still have been no reports on gas therapy for intracranial neuroglioma. Herein, an integrated, self-powered, and wirelessly controlled gas-therapy system is reported, which is composed of a self-powered triboelectric nanogenerator (TENG) and an implantable nitric oxide (NO) releasing device for intracranial neuroglioma therapy. In the system, the patient self-driven TENG converts the mechanical energy of body movements into electricity as a sustainable and self-controlled power source. When delivering energy to light a light-emitting diode in the implantable NO releasing device via wireless control, the encapsulated NO donor *s*-nitrosoglutathione (GSNO) can generate NO gas to locally kill the glioma cells. The efficacy of the proof-of-concept system in subcutaneous 4T1 breast cancer model in mice and intracranial glioblastoma multiforme in rats is verified. This self-powered gas-therapy system has great potential to be an effective adjuvant treatment modality to inhibit tumor growth, relapse, and invasion via teletherapy.

1. Introduction

Glioblastoma is the most aggressive and lethal type of tumor of the central nervous system.^[1] Due to the unique physiological anatomical features of the brain and the presence of the blood–brain barrier (BBB) and blood–brain tumor barrier (BBTB), few drugs can be efficiently delivered into the tumor tissues for efficient postoperative chemotherapy.^[2] As an alternative to chemotherapy, the emerging gas therapy has attracted

the attention of many researchers and is recognized as a kind of “green” therapeutic modality with high efficiency and low side effect.^[3] Several gas molecules, including nitric oxide (NO),^[4] carbon monoxide (CO),^[5] sulfur dioxide (SO₂),^[6] and hydrogen sulfide (H₂S),^[7] have been utilized for suppressing cancer cell growth. Among the family of gas molecules with therapeutic capacities, NO is the first gas transmitter considered to be a biological mediator, playing the most important roles in regulating physiological and pathophysiological activities such as neuronal communication,^[8] vascular regulation,^[9] and wound healing.^[10] Interestingly, high concentrations of NO (>1 × 10⁻⁶ M) can directly kill cancer cells through multiple pathways, including induction of cellular oxidative and nitrosative stress and mitochondrial/DNA damage, deamination of DNA bases, inhibition of DNA synthesis/repairing and cellular respiration, and enhancement of inflammatory

response.^[11] Due to the highly reactive nature and extremely short half-life (1.5–6 min) of NO, many nanoplatforms and nanocarriers have been fabricated for delivering stimuli-responsive NO donors, including nitroglutathione (GSNO),^[3a,12] *s*-nitrothiol,^[13] and Roussin's black salt^[14] into target tissues and releasing NO under the exogenous stimuli of heat,^[15] light,^[3a] X-ray,^[16] and ultrasound,^[17] etc., and endogenous stimuli of reactive oxygen species (ROS),^[18] pH,^[19] and H₂O₂.^[20] However, although great efforts have been devoted to designing

S. Yao, M. Zheng, Z. Wang, Y. Zhao, S. Wang, Z. Liu, Z. Li, Z. L. Wang, L. Li
Beijing Institute of Nanoenergy and Nanosystems
Chinese Academy of Sciences
Beijing 101400, P. R. China
E-mail: lilinlin@binn.cas.cn

S. Yao, Z. Liu, Z. Li, Z. L. Wang, L. Li
School of Nanoscience and Technology
University of Chinese Academy of Sciences
Beijing 101400, P. R. China

M. Zheng, Y. Zhao, S. Wang, Z. Li, Z. L. Wang, L. Li
Center on Nanoenergy Research
Guangxi University
Nanning 530004, P. R. China

Y. Guan
Cell Therapy Center
Beijing Institute of Geriatrics
Xuanwu Hospital
Capital Medical University
Beijing 100053, P. R. China
E-mail: guanyunqian@xwhosp.org

Z. L. Wang
School of Materials Science and Engineering
Georgia Institute of Technology
Atlanta, GA 30332-0245, USA
E-mail: zhong.wang@mse.gatech.edu

 The ORCID identification number(s) for the author(s) of this article can be found under <https://doi.org/10.1002/adma.202205881>.

DOI: 10.1002/adma.202205881

the nanocarriers and nanoplatfoms, there are still few reports on delivery of the NO donors across BBB with high efficiency. Moreover, it is also unfeasible to exert the exogenous stimuli with limited tissue penetration on the intracranial tumors with a high spatiotemporal precision.

Implantable optoelectronic devices have become powerful medical tools for diagnostic and therapeutic purposes, such as pacemakers, spinal cord stimulators, and deep brain stimulators.^[21] For neuroglioma, carmustine wafer implant (Gliadel wafer) is a clinically approved implantable device for the sustainable release of chemotherapeutic drug carmustine. More recently, Kennedy and co-workers developed an implantable upconversion nanoparticles-based implant that can convert near-infrared light into visible light to stimulate photosensitizer for photodynamic therapy of glioma.^[22] These examples have demonstrated the feasibility of direct implantation of a device during surgery for locoregional treatment, with increased efficacy and decreased systematic toxicity. However, for realizing locoregional gas therapy of deep-seated glioma, a convenient and continuous energy supply for stimulating gas generation is needed. The commonly applied wireless power supply requires an energy transmission device with a limited operating range, which might bring time and space constraints to the patients. In addition, wireless coils that receive energy in the living body may induce thermal damage to the surrounding normal tissues. Up to now, there have been no reports on intracranial implantable electronic devices for gas therapy.

For this decade, the burgeoning self-powered energy harvesting and conversion technologies of triboelectric nanogenerators (TEGs) provide a new opportunity and efficient pathway for self-powered biomedical applications. The wearable or implantable TEGs can efficiently harvest mechanical energy in the daily movement of humans, such as body movement, heartbeat, and respiration, and convert these energies into electricity.^[23] With these capacities, TEGs have been used for a series of self-powered biomedical diagnostic and therapeutic applications, including biosensing,^[24] drug delivery,^[25] tissue repairing,^[26] and self-powered cardiac pacing.^[27] Also, for the self-powered biomedical applications, TENG has the following advantages. First, TENG not only has the advantages of simple fabrication and flexible structure, but also, due to its wearable features, patients can rely entirely on their own natural movements to achieve energy harvesting and therapy manipulation. Second, TENG has good stability, long service life and can be powered for a long time without regular replacement, which is more convenient for patients with better compliance. Third, TENG made of biocompatible materials has good biosafety, avoiding the possible hazards of battery breakage to human bodies and the environment. Therefore, we hypothesize that the wearable and self-powered TENGs as an efficient electrical energy supply could be converted into other forms of energy as an efficient stimulus for gas generation and intracranial neuroglioma therapy. It can provide a promising approach to overcome the poor compliance and limited power supply of traditional implantable optoelectronic devices.

Herein, we demonstrate an integrated and self-powered system for neuroglioma gas therapy (**Figure 1**). In the system, a self-driven, wearable, and stretchable single-electrode mode TENG (wsTENG) is attached to the human body (finger, arm,

leg, etc.) to collect the energy from the body movements for electrical energy supply. An implantable NO-releasing device (NO-LED) is transcranially implanted into the brain close to the tumor tissue. In the NO-LED device, a blue LED is embedded in the center of the poly(dimethylsiloxane) (PDMS) matrix with incorporated photosensitive NO donor of GSNO. When LED is lightened by wsTENG via wireless control, the device can sustainably release NO for gas therapy. The wsTENG-based power supply system has the advantages of flexible and deformable structure, light weight and comfortable for wearing, good stability, long-term power supply, and no need for repeated replacement compared with other energy sources. The therapy process can be wirelessly manipulated by the patient through a smartphone with pre-customized treatment regimens for controlling timing, duration, and dosing of NO releasing.

2. Results and Discussion

2.1. Fabrication and Performance of wsTENG

The self-powered, wearable, and stretchable single-electrode mode TENG (wsTENG) was prepared by injecting conductive LiCl solution as the liquid electrode into a sealed silicone rubber capsule (**Figure 2A**). The obtained single-electrode TENG was flexible, highly stretchable and deformable, which was practicable for harvesting human mechanical energy when attached to the skin (**Figure 2B**). In addition, we tested the mechanical and tensile properties of wsTENG to demonstrate its structural stability. The wsTENG can be stretched up to 2420% with a tensile strength of up to 0.69 MPa (**Figure S2A**, Supporting Information). It also had good resilience after 15 tensile cycles of consecutive loading–unloading under the strains of 100% and 200% (**Figure S2B**, Supporting Information). After the consecutive loading–unloading, the voltage output of the wsTENG was almost unchanged (**Figure S2C**, Supporting Information). These results indicated that the TENG had good interfacial structural stability and can maintain good structural stability during large deformation, which will be beneficial to the extension of the lifetime of wsTENG. The initial size of wsTENG was 310 × 60 mm with the weight of only 58.5 g, being very lightweight and comfortable for wearing. The working mechanism of wsTENG is shown in **Figure 2C**. For the single-electrode TENG, the human skin acts as the ground. According to the triboelectric charging sequence, silicone rubber is an electronegative frictional electric material relative to human skin.^[28] When the skin comes in contact with silicone rubber, electrons are transferred from the skin to the surface of the silicon rubber. With the increased separation distance between skin and the silicon rubber, the negative charges on the rubber surface further induce positive charges in the LiCl electrolyte, driving the flow of free electrons from LiCl to the reference electrode. This electrostatic induction process can give an output voltage/current signal to the load. When the negative frictional charges on the silicone rubber are completely shielded by the induced positive charges of LiCl, the output signal returns to zero. When skin approaches the silicone rubber again, the induced positive charges in LiCl decrease and electrons flow from the reference electrode to LiCl, until the skin and the silicone rubber are in

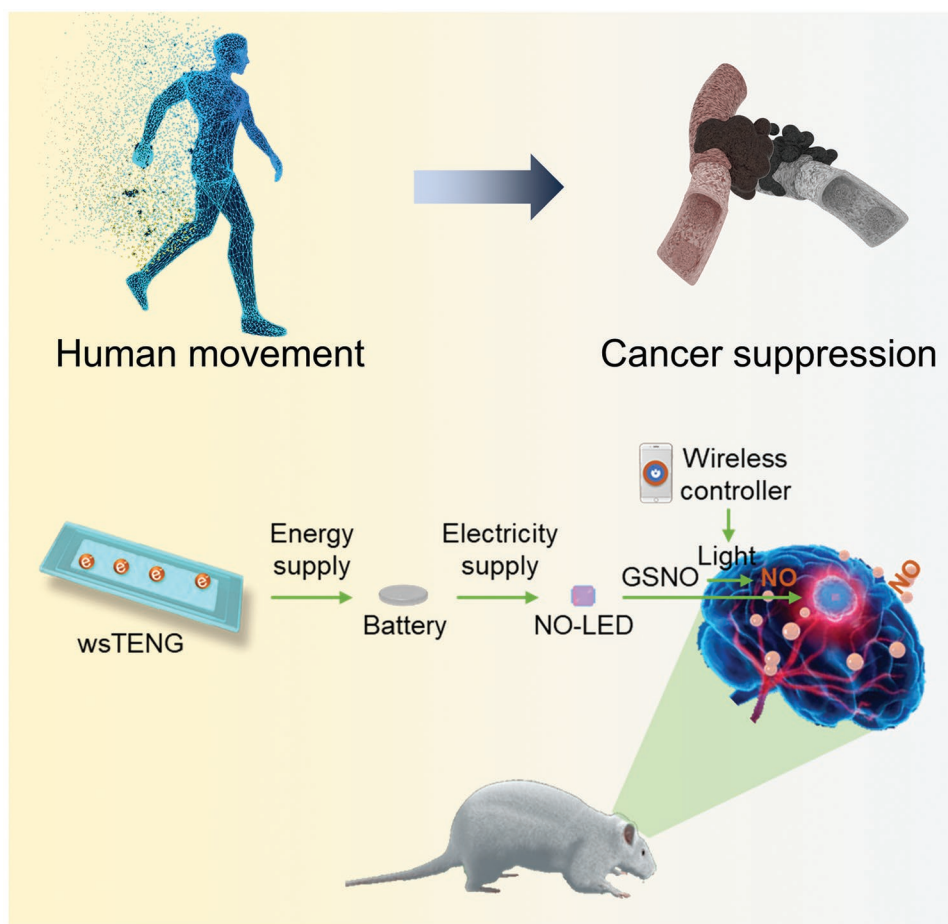


Figure 1. Schematic diagram of intracranial glioblastoma therapy with the self-powered wsTENG-based NO gas-therapy system.

full contact again, resulting in a reverse output signal. This is a complete cycle of the power generation process.

To explain the working mechanism of wsTENG, the spatial potential distribution during the periodic contact–separation between the skin and the silicone rubber layer was simulated using COMSOL. The change of the potential difference between skin and the silicone rubber shows the same trend as deduced (Figure 2D). Then, the output performance of wsTENG was detected under the mechanical forces in the vertical direction. The alternating voltage and current were generated by cycling the contact–separation processes between a volunteer’s finger and the silicone rubber. The open-circuit voltage (V_{oc}) peaked at ≈ 395 V, and the short-circuit current (I_{sc}) reached ≈ 2.3 μ A when the finger’s motion frequency was 1 Hz (Figure 2E,F). After about 1800 cycles of friction within 1800 s, the V_{oc} value remained stable at ≈ 401 V (Figure 2G). In addition, the wsTENG output remained almost unchanged after 21 d (Figure S3, Supporting Information), indicating that the wsTENG had good stability and long service life. To investigate the output of wsTENG under nonconstant strain rate, we tested the output voltage of the wsTENG at different friction frequencies (Figure S4, Supporting Information). The experimental results showed that wsTENG was able to stabilize the output well at about ≈ 410 V during the variation of the friction

frequencies from 0.8 to 2.4 Hz, which are normal frequencies of human limb activities. It demonstrated that wsTENG can maintain a stable output under a nonuniform strain rate. We also tested the variation of current, voltage and power density of wsTENG under different load resistances (Figure 2H,I). As the load resistance increased from 1 k Ω to 1 G Ω , the output current decreased, and the output voltage increased accordingly. Under the matching resistance of 200 M Ω , the maximum power generated by wsTENG reached 680 μ W, corresponding to a power density of 30.35 mW m $^{-2}$. We further assembled a self-charging power system using wsTENG as the self-powered power source. The wsTENG was driven by human arm bending, and a button battery (3 V, 18 mAh) or a capacitor was assembled by power management to form the self-charging power system (Figure 2J), which can power an electronic watch, or a temperature sensor (Figure 2K; Videos S1 and S2, Supporting Information). The electrical energy harvested from the arm bending in about 60 s can simultaneously drive an electronic watch to work for about 20 s. The button battery can be charged from 1.8 to 2.5 V by wsTENG in 12 h, and discharged from 2.5 to 1.65 V when being connected with a blue LED (Figure 2L,M), which continuously lightened the LED for 2 h. It demonstrated the great potential for the self-powered wsTENG-based e-medical device.

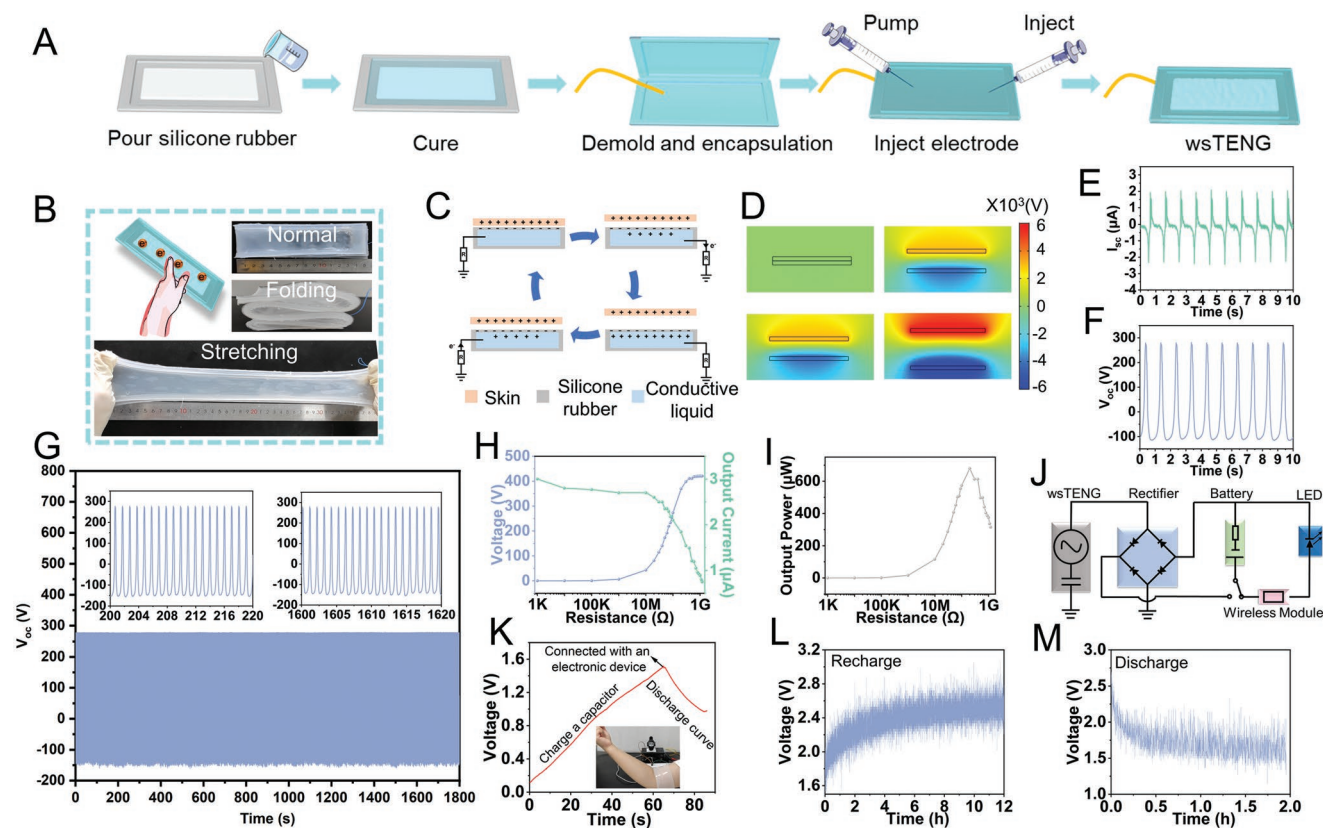


Figure 2. Fabrication, output, and energy harvesting performance of the wearable and stretchable single-electrode mode TENG (wsTENG). A) Schematic illustration of the detailed fabrication process of wsTENG. B) Schematic illustration of wsTENG and photographs of the as-prepared wsTENG under different states including normal, folding and stretching. C) A cycle of electricity generation process of wsTENG. D) Finite element simulation via COMSOL for analyzing the potential distribution during friction. E) I_{sc} and F) V_{oc} of wsTENG under finger friction within 10 s. G) V_{oc} output stability of wsTENG within 1800 s. Inset shows V_{oc} within 20 s. H) The output current and voltage with the resistance of external loads. I) The output power with the resistance of the external loads. J) Equivalent circuit of the self-charging power system to power a blue LED. K) Charging and discharging curves of a capacitor connected with power management. Inset shows driving of an electronic watch. L) Charging and M) discharging curve of a button battery by wsTENG.

2.2. Preparation and NO Releasing Performance of NO-LED

To fabricate the NO-releasing device NO-LED, a blue LED (3 mm in length, 1.5 mm in width, and 0.8 mm in height) was encapsulated into a PDMS matrix containing photosensitive NO donor of GSNO (10 mg mL^{-1}) before the polymerization of PDMS prepolymer (Figure 3A). The NO-LED device with a final dimension of $4 \times 3.5 \times 2.5 \text{ mm}$ was obtained after curing and demolding (Figure 3B, insert). The coating made of PDMS is elastic and flexible to match the soft tissues.^[29] When NO-LED was connected with the self-charging power system based on wsTENG, the blue LED can be lightened continuously (Figure 3B), and the blue light with a wavelength of 455–465 nm can further stimulate GSNO for continuous NO generation. The connection details of the wirelessly controllable self-powered NO release device are shown in Figure 3C. Next, we evaluated the sealing stability of PDMS. The experimental results showed that the NO-LED emitted light normally during the 21-d of immersion in the simulated body fluid, indicating that PDMS had good sealing performance (Figure 3D). On the contrary, when LED was not

well-encapsulated, the luminous performance of LEDs was greatly diminished.

We also evaluated the NO releasing ability from NO-LED under different light luminous intensities. When NO-LED was immersed in phosphate buffer solution (PBS) without light illumination, the release of NO into the medium was negligible within 30 min (Figure 3E). When the LED in NO-LED was lightened by wsTENG with a luminous intensity of 0.3 mW cm^{-2} , NO was continuously generated and diffused from the PDMS matrix into the PBS medium, reaching an accumulative concentration of $274 \times 10^{-6} \text{ M}$ in 30 min (Figure 3E). To illustrate the longevity of NO-LED, we tested the NO release from the NO-LED during 20 cycles of LED light irradiation (0.3 mW cm^{-2} , 30 min for each cycle). The experimental results showed that after 20 cycles, the NO-LED can still sustainably release NO with a concentration of $19.05 \times 10^{-6} \text{ M}$ (vs $274 \times 10^{-6} \text{ M}$ of the 1st cycle). And the consumed GSNO in the 20 cycles was about 16.1% of the loaded GSNO in NO-LED (Figure S9, Supporting Information). It proved that the device can support long-term tumor treatment. As a control, we tested lightening of the NO-LED by a normal miniature coin cell (3 V). We found that

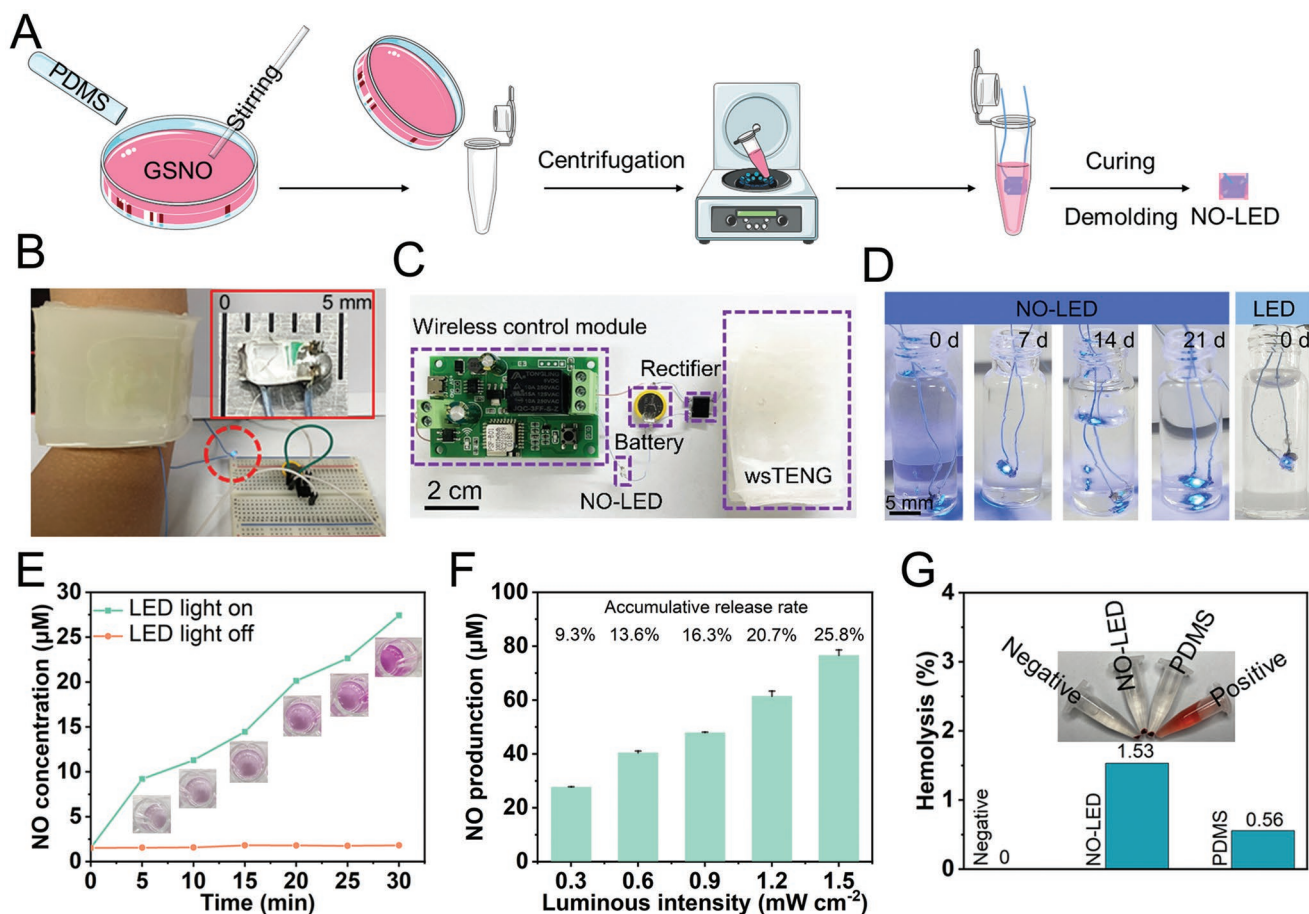


Figure 3. Preparation and NO releasing performance of NO-LED. A) Schematic illustration of the fabrication process of NO-LED. B) Photograph showing lightening of NO-LED by wsTENG in ambient environment. C) Photograph showing the whole therapeutic system with the circuit configuration. D) The luminescence of NO-LED and LED without PDMS coating when immersed in simulated body fluids for different times. E) NO generation from NO-LED with and without light irradiation enabled by wsTENG. Inset shows the color development of the NO assay kit at different irradiation times. F) NO production in 30 min with different LED luminous intensities. G) Hemolytic rate of defibrinated sheep blood under different conditions (negative control, NO-LED device, blank PDMS device, and positive control).

after 2 cycles of continuous power supply by the miniature coin cell, its voltage was significantly weakened (Figure S10, Supporting Information). And after 2 cycles, only 20.1×10^{-6} M of NO was produced by the NO-LED, while 27.12×10^{-6} M of NO was produced by the NO-LED powered by wsTENG; after 20 cycles, the released NO greatly dropped to 13.16×10^{-6} M. With the luminous intensities increased from 0.3 to 1.5 mW cm^{-2} , the NO production was enhanced accordingly from 27.4 to 76.6×10^{-6} M in 30 min, with the highest release rate of 25.8% calculated from the molar weight of GSNO (Figure 3F).

Moreover, the device had high hemocompatibility with a low hemolysis (1.53%) after the coincubation with the defibrinated sheep blood for 6 h (Figure 3G). Even when the LED light was on, the blank PDMS+LED pseudo device had high hemocompatibility with a low hemolysis (1.45%) after light irradiation of the defibrinated sheep blood for 6 h (Figure S6, Supporting Information). Therefore, the use of wsTENG to power the NO-LED has the advantages of good stability, long service life, long-term power supply, no need for regular replacement, convenience for patients, and better compliance.

2.3. In Vitro Cancer Therapy

With the controllable NO releasing property, we further examined the anticancer effect of the system at the cellular level. First, the cytocompatibility of the device was evaluated on mouse fibroblast NIH-3T3 cells. After coincubation of the NIH-3T3 cells with NO-LED immersed in the culture media for 24 h, the cells still had viability close to 100% via 3-(4,5-dimethylthiazol-2-yl)-2,5-diphenyltetrazoliumbromide (MTT) assay (Figure 4A). Then, we verified the therapeutic effect of NO releasing by GSNO on the mouse breast cancer cell 4T1 and rat glioma cell C6. The cells were cocultured with different concentrations of GSNO (1.56 – $100 \mu\text{g mL}^{-1}$) and exposed to LED light (0.3 mW cm^{-2}) for 30 min, and the cell viability after 24 h additional culture was evaluated. The results showed that without LED light irradiation, both the 4T1 and C6 cells had high viability, close to 100%, even under the high GSNO concentration of $100 \mu\text{g mL}^{-1}$ (Figure 4B,C). With the presence of LED light irradiation, the 4T1 and C6 cells incubated with GSNO had reduced cell viability along with increased GSNO concentrations. When the

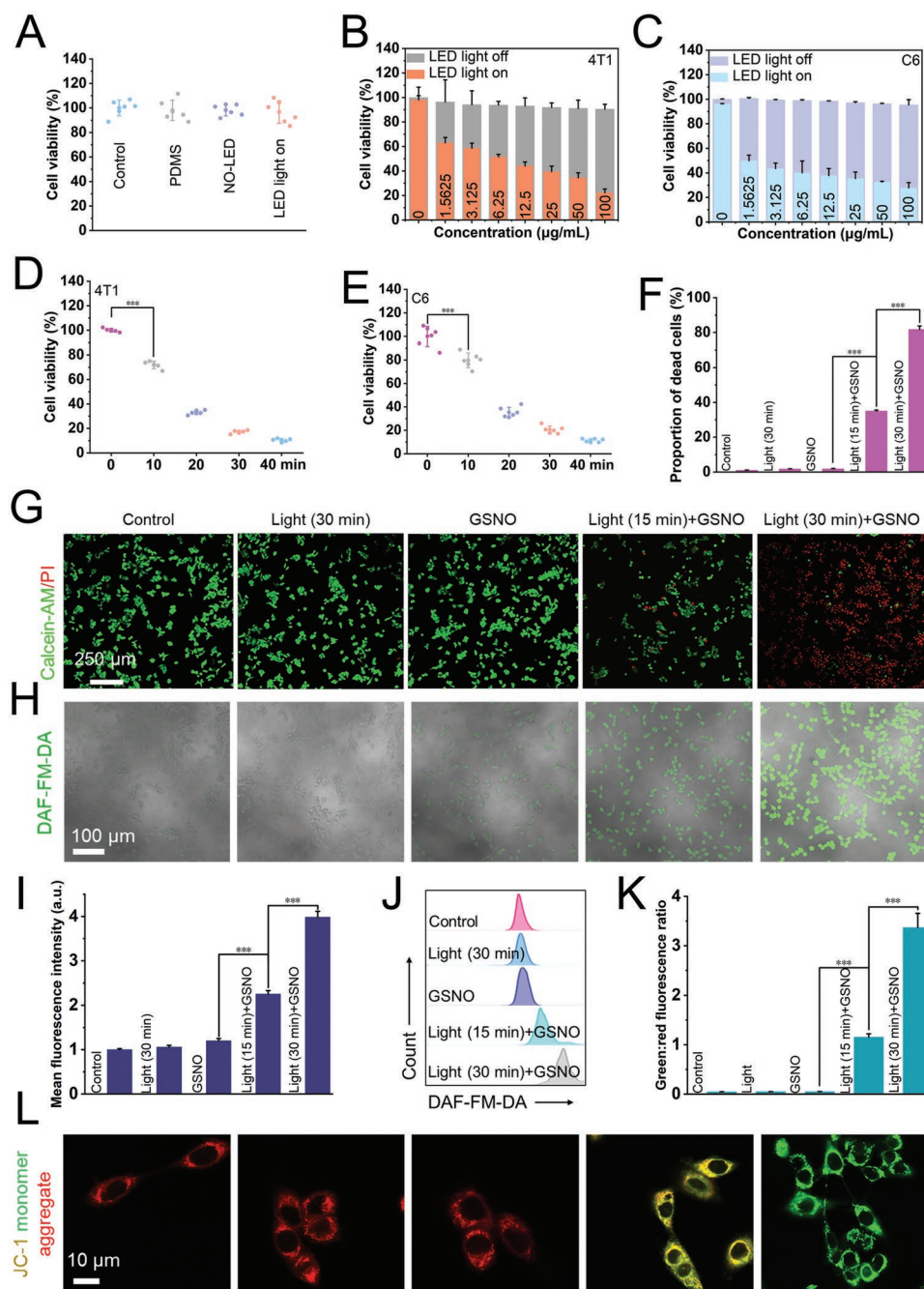


Figure 4. In vitro cancer therapeutic effect of NO-LED. A) Viability of 3T3 cells after different treatments for 24 h. B, C) Viability of 4T1 (B) and C6 (C) cells after different treatments for 24 h. D, E) Viability of 4T1 (D) and C6 (E) cells incubated with NO-LED and light-irradiated for different times. F, G) The C6 cells co-stained with Calcein-AM (green fluorescence) and PI (red fluorescence) and corresponding statistic result of dead cell percent. H, I) Confocal imaging of NO generation in C6 cells stained by DAF-FM-DA. The photos are merged from green fluorescence images and corresponding bright-field images. The statistic result shows the relative mean fluorescence intensity under the different treatments with fluorescence of the control group setting as 1. J) Flow cytometry analysis of the C6 cells stained with DAF-FM-DA after the treatment with Light, GSNO and Light + GSNO (15 or 30 min) to evaluate the intracellular NO production. K, L) Confocal images merged from green and red channels showing JC-1 staining of the C6 cells after different treatments. The statistic result shows the green: red fluorescence ratio under different treatments. The asterisks (*) denote statistical significance between the bars. $P < 0.05$ is considered to be statistically significant, conducted using GraphPad Prism 6.0. *** represents $P < 0.001$.

concentration of GSNO was $100 \mu\text{g mL}^{-1}$, the cell survival rate of the 4T1 and C6 cells reduced to 22.3% and 27.8%, respectively. We further determined the killing effect of the NO-LED device on 4T1 and C6 cells. From the results of the 4T1 cells incubated

with NO-LED with different light irradiation times (Figure 4D), the survival rate of the 4T1 cells decreased with prolonged light irradiation times and was only 10.3% after 40 min of light irradiation. For the C6 cells incubated with NO-LED with different

light irradiation times (Figure 4E), the survival rate of the C6 cells was only 20.4% and 11.3% after 30 and 40 min of light irradiation, respectively. The live-dead cell staining showed similar results. In the mere Light (30 min) and GSNO (100 $\mu\text{g mL}^{-1}$) groups, only 1.6% and 1.8% of the C6 cells were killed, respectively. In contrast, in the Light+GSNO (30 min) group, most of the cells were dead (84%) (Figure 4F,G).

After different treatments of the C6 cells, the intracellular NO levels were detected using 4-amino-5-methylamino-2',7'-difluorofluorescein diacetate (DAF-FM-DA) as a NO indicator. As shown in Figure 4H,I, the cells after treatments with Light+GSNO for 15 and 30 min showed increased intracellular green fluorescence, whose relative intensity had a 1.58 and a 2.23-fold increase compared to the control group, respectively. The same results were obtained by flow cytometry (Figure 4J). We further examined the changes in cellular mitochondrial membrane potential (MMP) after different treatments using 5,5',6,6'-tetrachloro-1,1',3,3'-tetraethylimidazolium cyanide (JC-1) as the specific indicator. The change in MMP is the main indicator of mitochondrial dysfunction and cellular oxidative damage. It can be reflected by the change in the green:red fluorescence ratio of JC-1, where the green fluorescence is from the

monomeric forms representing low MMP and the red fluorescence is from the J-aggregates representing high MMP. The cells in the several negative control groups, including the control, Light, and GSNO groups showed mainly red fluorescence, and their green fluorescence signals were almost negligible (Figure 4K,L). In contrast, the cells in the Light+GSNO (15 min) and Light+GSNO (30 min) group showed strong green fluorescence, while the Light+GSNO (30 min) showed the highest green:red fluorescence ratio with a 63.3-fold increase relative to the control group, suggesting the occurrence of cellular mitochondrial oxidative damage.

2.4. In Vivo Cancer Therapy in Subcutaneous 4T1-Tumor-Bearing Mice

The performance of the self-powered wsTENG-based NO gas-therapy system was verified through in vivo cancer therapy. The subcutaneous 4T1 tumors on BALB/c mice were first used to study the therapeutic effect (Figure 5A). Before therapy, we firstly verified the biocompatibility of wsTENG attached to the human body. The morphology of mouse fibroblast L929 had

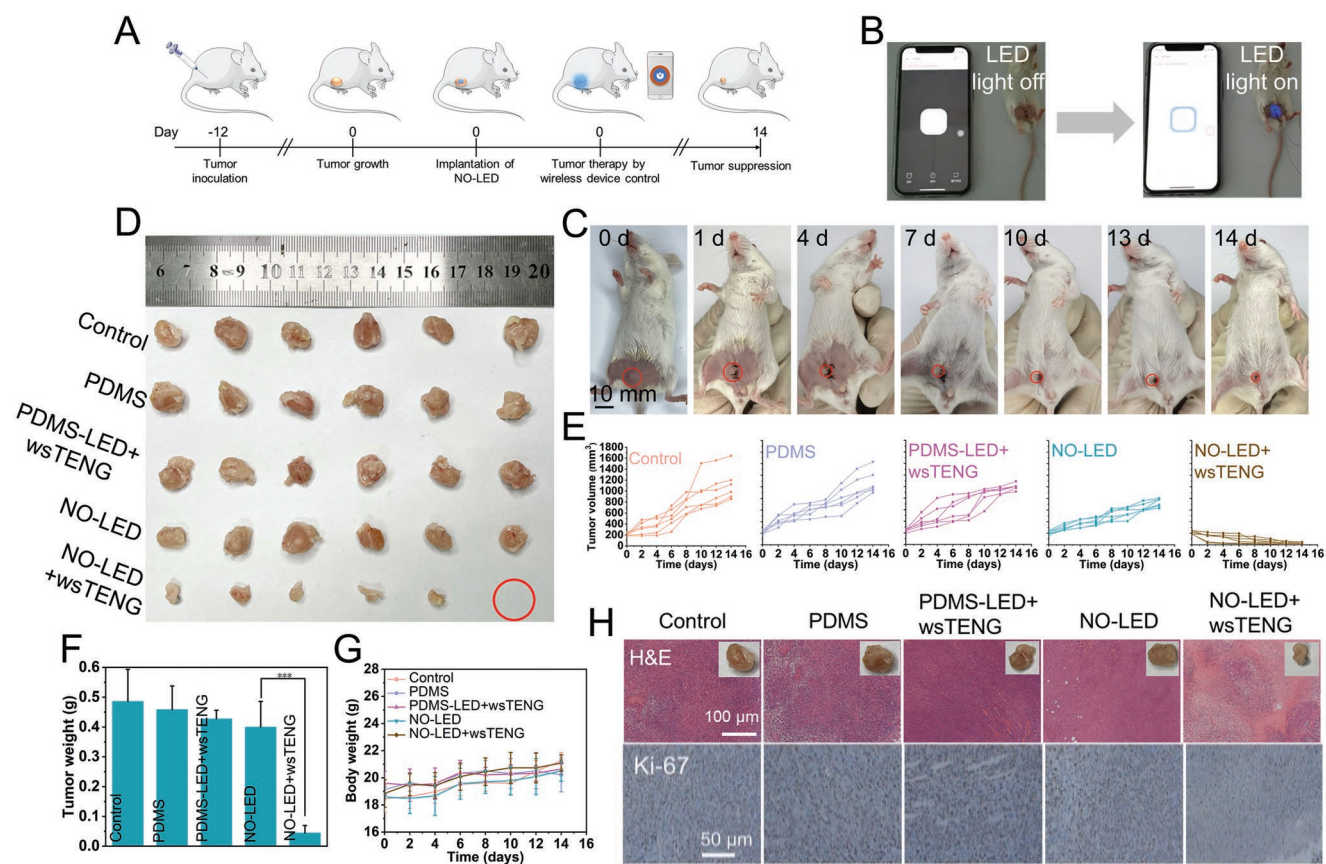


Figure 5. In vivo cancer therapy on the subcutaneous 4T1-tumor-bearing BALB/c mice with the self-powered wsTENG-based NO gas-therapy system. A) Schematic illustration of the cancer therapy. B) Photographs of NO-LED turn-on/off by wireless control using a smartphone. C) Photographs of the representative mouse in the NO-LED + wsTENG group during the 14 d of treatment. The red circle areas in the photos shows the location and size of the tumor tissue. D) Photographs of the representative stripped tumor tissues at the terminal of the therapy. E) Tumor volume change of the mice during the treatment. F) Mean tumor weights after the excision of the tissues at day 14. G) Body weight change of the mice during the treatment. H) H&E and Ki-67 staining of the tumor tissues.

no obvious change after 24 h coculture of the cells with Ecoflex, which was the directly contacted layer of wsTENG with the human skin (Figure S7, Supporting Information). The result indicated that the device had good biocompatibility.

Next, the tumor-bearing mice with the tumor size of 100–200 mm³ were randomly divided into five groups ($n = 6$): (1) a control group; (2) a PDMS group, implanted with a blank PDMS pseudo device next to the tumor tissues; (3) a PDMS-LED + wsTENG group, implanted with a blank PDMS+LED pseudo device without GSNO and light-stimulated via wsTENG; (4) a NO-LED group, implanted with NO-LED; (5) a NO-LED + wsTENG group, implanted with NO-LED and light-stimulated via wsTENG. Details of these groups were provided in the experimental section. The NO-LED, pseudo PDMS or PDMS-LED devices were implanted subcutaneously near the tumor tissues and connected with wsTENG attached to a human arm. For executing the wsTENG-enabled light stimulation, the system was wirelessly manipulated via a smartphone (Figure 5B; Videos S3 and S4, Supporting Information). The stimulation was performed for only once and lasted for 30 min. At the end of the 14-d of therapy, the mice tumors in the NO-LED + wsTENG group were completely eradicated for one out of the total six mice, and the tumor growth was significantly inhibited for the other five mice (Figure 5C–F). The tumor inhibition rate was calculated to be 90.9% at the end of the therapy. In contrast, the tumor growth in the PDMS, PDMS-LED + wsTENG group, and NO-LED group was almost not inhibited with the tumor inhibition rates of only 5.6%, 12.1%, and 177%, respectively. During the treatment, there was no significant change in the body weight of the mice in all the groups, suggesting high biocompatibility of the therapeutic process (Figure 5G). Further histopathological analysis, including hematoxylin and eosin (H&E) staining and Ki-67 immunohistochemistry of the tumor tissues confirmed the results (Figure 5H). These results demonstrated that the excellent therapeutic effect of the implantable NO-LED device was mainly attributed to the NO releasing from the device under the wsTENG-enabled light stimulation.

2.5. In Vivo Cancer Therapy of Intracranial C6 Glioma in SD Rats

We further investigated the therapeutic ability of the system on intracranial C6 gliomas in SD rats (Figure 6A). The rats were divided into four groups ($n = 2$): (1) a control group, (2) a PDMS-LED + wsTENG group, (3) a NO-LED group, and (4) a NO-LED + wsTENG group. NO-LED or pseudo PDMS-LED devices was implanted intraoperatively during the construction of the tumor models to avoid secondary surgery. After the NO-LED implantation and surgical suture, the therapy was initiated wirelessly using a smartphone. The stimulation was executed for only one time and lasted for 30 min. During the therapy, the tumor progression and tumor volume change were monitored through microcomputed tomography (micro-CT) imaging (Figure 6B; Figure S16, Supporting Information). The white dashed lines in the photographs and the pseudo-color images indicated the density distribution of the intracranial tumors. In the NO-LED + wsTENG group, the tumor density distribution gradually decreased along with time, indicating

that the malignancy of the tumors gradually decreased. The tumors were almost invisible on day 21, and the rats survived well after 21 d, indicating that the self-powered and wirelessly controlled NO releasing had a good cancer-inhibiting effect. In contrast, the inhibition of tumor growth by light irradiation alone (the PDMS-LED + wsTENG group) and the implanted NO-LED device without light irradiation (the NO-LED group) was negligible, and the rats in these groups all died during days 15–17 after the implantation of the C6 cells and the devices. The optical images of the tumor tissues (Figure 6B, insets at bottom right corner) as well as the corresponding H&E and Ki-67 staining also confirmed the high tumor-suppressive effect of the self-powered wsTENG-based NO gas therapy (Figure 6C). At the end of the therapy, the blood routine and blood biochemistry indexes had no obvious abnormality, suggesting high biocompatibility of the therapy (Figure 6D). From these results, the self-powered wsTENG-based NO gas therapy realized a wirelessly controlled light stimulation and NO releasing for intracranial tumor inhibition. It showed the advantages of self-driving, convenience, and controllability that are difficult to be realized through other modalities.

3. Conclusion

We have designed and fabricated a self-controlled wsTENG-based implantable self-powered NO generation system to realize the therapy of cancers, especially intracranial neuroglioma. The in vitro and in vivo experimental results confirm the efficient therapeutic outcome of the proof-of-concept system. In the system, wsTENG as a wearable and sustainable energy supply device can convert biomechanical energy of human movements into electrical energy, which exempts replacement of the power supply. The NO releasing device can be locally implanted during surgery, which improves the bioavailability and reduces systematic side effects. With a customized treatment regimen, the system can be self-controlled by the patients through a smartphone to switch on/off the LED light and therefore control the NO generation to meet different treatment requirements. This research might provide inspiration for the development of self-powered wearable/implantable bioelectronic devices and systems to improve patient compliance and realize teletherapy.

4. Experimental Section

Materials: Silicone rubber (Ecoflex 00-30 with agent A and agent B) was purchased from Smooth-On Inc. Anhydrous lithium chloride was purchased from Xilong Science Co., Ltd. PDMS (Sylgard184 Silicone Elastomer Kit with Part A and Part B) was purchased from Zork Biotechnology Development Co., Ltd. S-Nitrosoglutathione (GSNO) was purchased from Shanghai McLin Biochemical Technology Co., Ltd. (Shanghai, China). Calcein-acetoxymethyl ester (Calcein AM)/propidium iodide (PI) cell viability/cytotoxicity assay kit, MMP assay kit with JC-1 [5,5,6,6-tetrachloro-1,1,3,3-tetraethylbenzimidazolylcarbocyanine iodide], and 3-(4,5-dimethyl-2-thiazolyl)-2,5-diphenyl tetrazolium bromide (MTT) were purchased from Beijing Solarbio Science & Technology Co., Ltd. Nitric oxide assay kit and 4-amino-5-methylamino-2',7'-difluorofluorescein diacetate (DAF-FM-DA) were purchased from Beyotime Technology Co., Ltd. (Shanghai, China). Sheep blood samples

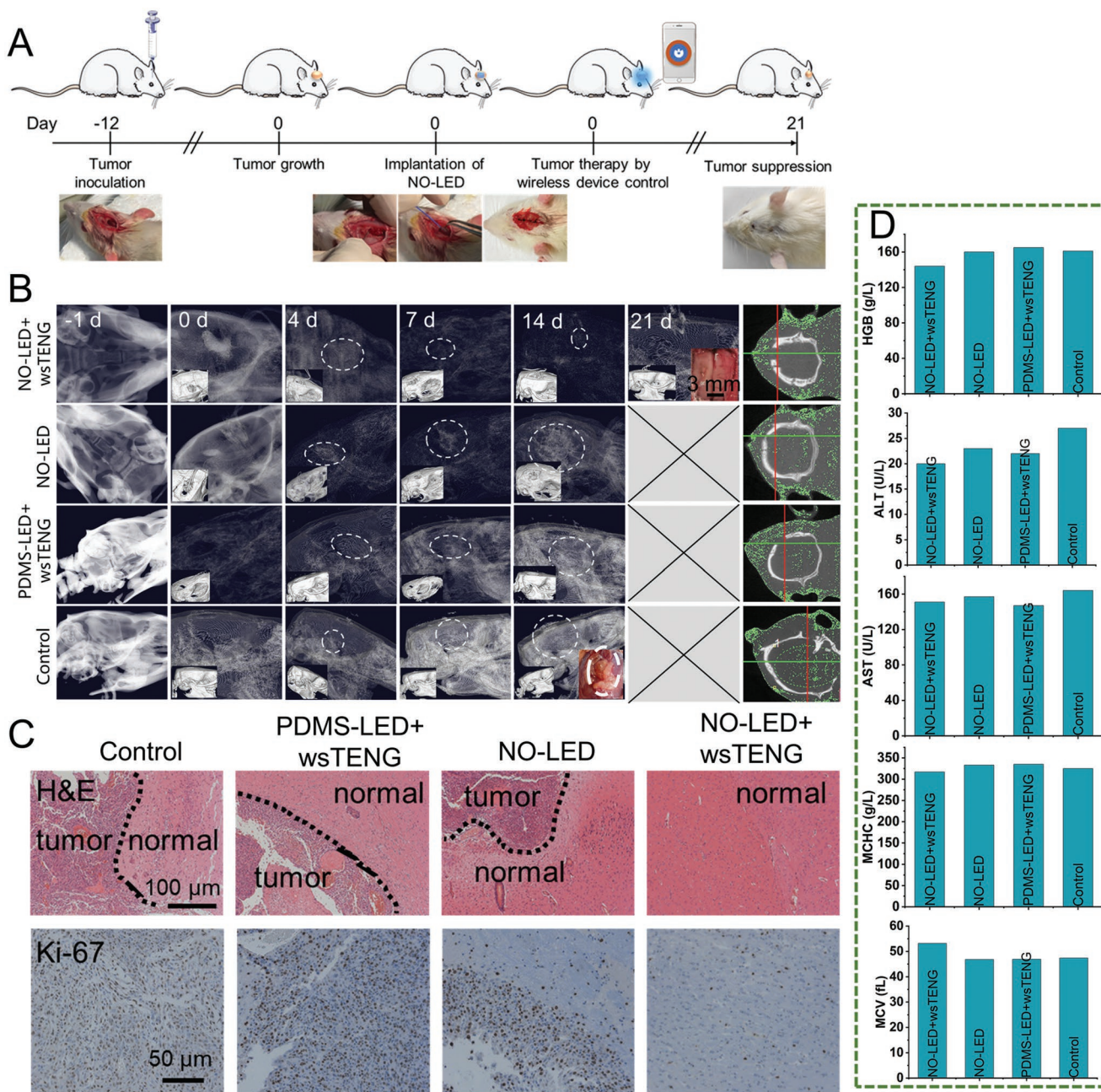


Figure 6. The therapy of intracranial C6 glioma in SD rats with the self-powered wsTENG-based NO gas therapy. A) Schematic illustration and corresponding photographs of the cancer therapy. B) Micro-CT contrast imaging of the rats during the treatment. The insets at lower left quarter show the basic outline of the rat skull, and the insets at the bottom right corner show the peeled brain tumors. The right pseudocolor maps in each group show the density distribution of the brain tumors. C) H&E histopathological and Ki-67 immunohistochemical staining of the tumor tissues. D) The blood routine and blood biochemistry examination of the mice after different treatments.

were acquired from Beijing Land Bridge Technology Co., Ltd. (Beijing, China).

Preparation of wsTENG: Anhydrous lithium chloride was dissolved in deionized water to form lithium chloride solution (0.1 g mL^{-1}) as the liquid electrode. A hollow structured silicone rubber capsule was fabricated with the assistance of an acrylic box ($315 \text{ mm} \times 65 \text{ mm}$) as the mold. A tape ($260 \text{ mm} \times 40 \text{ mm}$, thickness of 1 mm) was glued in the middle of the bottom of the acrylic box. The height of wsTENG's cavity was determined by the thickness of the tape. Then, the liquid made by mixing agent A with agent B ($v:v = 1:1$) was poured into the acrylic mold.

After curing at $65 \text{ }^\circ\text{C}$ for 2 h, the silicone rubber was demolded from the acrylic mold. Two identical pieces of silicone rubber were attached to each other face-to-face to form a cavity and the copper wires were inserted at the two terminals. Finally, the LiCl liquid electrode was injected into the cavity by a syringe and the residual air in the cavity was extracted by another syringe. The wsTENG was obtained with a whole thickness range of 3–4 mm.

Preparation of NO-LED: GSNO (10 mg) was stirred and mixed with 11 g PDMS prepolymer solution ($10:1$ w/w ratio of Part A to Part B). The mixture ($300 \text{ } \mu\text{L}$) was added into a starch capsule tube and a blue

LED ($3 \times 1.5 \times 0.8$ mm) were put at the center. The tube was heated at 37°C for 24 h under dark. Then, the device was detached from the mold through incubating the starch capsule tube in ultrapure water at 37°C . The final size of the device was $4 \times 3.5 \times 2.5$ mm. During the course, the connected wire was also encapsulated with PDMS.

Preparation and Implementation of the Self-Powered NO Gas-Therapy Systems: The self-powered NO gas-therapy system consisted of a wireless receiver module for electronic control, a NO-LED therapy module, and a wsTENG with the self-driven function connecting a miniature coin cell. For therapy, the miniature coin cell was firstly charged with the self-powered wsTENG driven by arm bending of the volunteer. Then, the power stored in the miniature button cell was used to power the NO-LED. The turning on/off of the NO-LED was wirelessly controlled through a smartphone.

In Vitro NO Generation Assay by DAF-FM-DA: The C6 cells after different treatments were stained with DAF-FM-DA ($1\text{ mL}, 5 \times 10^{-3}\text{ M}$) for 20 min and washed twice with PBS. Fluorescence of the cells was observed using a confocal laser scanning microscope (Leica, SP8).

Animals: BALB/c mice (female; 17–20 g) and SD rat (male; 270–320 g) were provided by Beijing Charles River Laboratories, and the procedures for handling the animals were performed firmly according to the national standards "Laboratory Animal Requirements of Environment and Housing Facilities" (GB 14925-2001). The animal experiments were approved by the Animal Experimental Ethical Inspection in Xuanwu Hospital of Capital Medical University (Approval Number: XW-20210423-2).

In Vivo Breast Cancer Therapy in BALB/c Mice: 4T1 cells (5×10^5 cells suspended in $100\ \mu\text{L}$ PBS) were injected into the subcutaneous region of the left lower abdomen of the mice. When the tumor volume reached $\approx 100\text{--}200\text{ mm}^3$, the mice were randomly divided into 5 groups ($n = 6$): (1) Control group: without any treatment; (2) PDMS group: implanted with blank PDMS pseudo device of the same size next to the tumor tissues; (3) PDMS-LED (without GSNO) + wsTENG group: implanted with PDMS-coated LED pseudo device and light-irradiated for 30 min enabled by wsTENG; (4) NO-LED group: implanted with NO-LED without light irradiation; (5) NO-LED + wsTENG group: implanted with NO-LED and light-irradiated for 30 min enabled by wsTENG. For executing the wsTENG-enabled light stimulation, the system was wirelessly manipulated via a smartphone. wsTENG was attached on the volunteer's arm and the electrical signal was outputted under the arm swing. The stimulation was executed for only one time and lasted for 30 min. Throughout the experimental period, each mouse was labeled and followed individually. Tumor volume and body weight were recorded until euthanasia. After 14 d of treatment, the mice were executed and the major organs including heart, liver, spleen, lung, kidney, and tumors were peeled for further pathological analysis by H&E staining and Ki-67 immunohistochemistry (for tumor tissue only). The blood routine and blood biochemistry of the 4T1 bearing BALB/c mice were examined after different treatments. All the participants driving wsTENG consented to the experiments.

In Vivo Glioma Therapy in SD Rats: For the therapy of SD rat gliomas, the suspension of C6 cells (2×10^6 cells in $10\ \mu\text{L}$ PBS) was slowly injected into the right corpus striatum (1.8 mm lateral, 0.6 mm anterior to the bregma, and 3.0 mm in depth) of the rats by a stereotactic fixation device using a mouse adaptor. When the tumor contrast of the rat brain appeared observed through micro-CT (Quantum GX), the rats were randomly divided into 4 groups ($n = 2$): (1) Control group without any treatment; (2) PDMS-LED + wsTENG group: implanted with PDMS-coated LED pseudo device and light-irradiated for 30 min enabled by wsTENG; (3) NO-LED group: implanted with NO-LED without light irradiation; (4) NO-LED + wsTENG group: implanted with NO-LED and light-irradiated for 30 min enabled by wsTENG. For NO-LED intracranial implantation, a $D = 3.5$ mm notch in the right coronal sulcus (1.8 mm laterally and 0.6 mm anterior to fontanelle) of the rat was drilled through a motorized cranial drill, and the NO-LED was implanted into the cranium and the surgical wound was sutured. The wsTENG was attached on the volunteer's arm and the electrical signal was outputted under the arm swing. For executing the wsTENG-enabled light stimulation, the

system was wirelessly manipulated via a smartphone. The stimulation was executed for only one time and lasted for 30 min. Throughout the experimental period, each rat was tagged and tracked individually. The rat body weight was recorded until euthanasia. After 21 d of treatment, the rats were executed and the tumors were obtained for further pathological analysis by H&E staining and Ki-67 immunohistochemistry. The blood routine and blood biochemistry of the rats were examined after different treatments. All the participants driving wsTENG consented to the experiments.

Statistical Analysis: All data are expressed as mean \pm s.d. error. Statistical differences between different groups of data were evaluated by one-way analysis of variance, and $p < 0.05$ was considered statistically significant. The asterisks (*) denote the statistical significance between bars (* $p < 0.05$, ** $p < 0.01$, and *** $p < 0.001$) conducted using GraphPad Prism 6.0.

Supporting Information

Supporting Information is available from the Wiley Online Library or from the author.

Acknowledgements

The work was supported by the Strategic Priority Research Program of the Chinese Academy of Sciences (No. XDA16021103), the National Nature Science Foundation (No. 82072065, 81471784), the National Youth Talent Support Program and the China Postdoctoral Science Foundation (Nos. BX2021299, 2021M703166), the National Youth Talent Support Program, and the Fundamental Research Funds for the Central Universities (E2EG6802X2, E2E46801).

Conflict of Interest

The authors declare no conflict of interest.

Data Availability Statement

The data that support the findings of this study are available from the corresponding author upon reasonable request.

Keywords

gas therapy, implantable devices, neuroglioma, self-powered devices, wireless control

Received: June 28, 2022
Revised: September 27, 2022
Published online:

- [1] a) W. Niu, Q. Xiao, X. Wang, J. Zhu, J. Li, X. Liang, Y. Peng, C. Wu, R. Lu, Y. Pan, J. Luo, X. Zhong, H. He, Z. Rong, J. B. Fan, Y. Wang, *Nano Lett.* **2021**, *21*, 1484; b) J. Li, J. Kong, S. Ma, J. Li, M. Mao, K. Chen, Z. Chen, J. Zhang, Y. Chang, H. Yuan, T. Liu, Z. Zhang, G. Xing, *Adv. Funct. Mater.* **2021**, *31*, 2100969; c) L. van Hooren, A. Vaccaro, M. Ramachandran, K. Vazaios, S. Libard, T. van de Walle, M. Georganaki, H. Huang, I. Pietila, J. Lau, M. H. Ulvmar, M. C. I. Karlsson, M. Zetterling, S. M. Mangsbo, A. S. Jakola,

- T. Olsson Bontell, A. Smits, M. Essand, A. Dimberg, *Nat. Commun.* **2021**, *12*, 4127.
- [2] a) S. Pinel, N. Thomas, C. Boura, M. Barberi-Heyob, *Adv. Drug Delivery Rev.* **2019**, *138*, 344; b) W. Tang, W. Fan, J. Lau, L. Deng, Z. Shen, X. Chen, *Chem. Soc. Rev.* **2019**, *48*, 2967; c) J. Feng, S. Lepetre-Mouelhi, A. Gautier, S. Mura, C. Cailleau, F. Coudore, M. Hamon, P. Couvreur, *Sci. Adv.* **2019**, *5*, eaau5148.
- [3] a) B. Li, P. Ji, S. Y. Peng, P. Pan, D. W. Zheng, C. X. Li, Y. X. Sun, X. Z. Zhang, *Adv. Mater.* **2020**, *32*, 2000376; b) L. Chen, S. F. Zhou, L. Su, J. Song, *ACS Nano* **2019**, *13*, 10887; c) W. Fan, B. C. Yung, X. Chen, *Angew. Chem., Int. Ed.* **2018**, *57*, 8383; d) Y. Opoku-Damoah, R. Zhang, H. T. Ta, Z. P. Xu, *Exploration* **2022**, *2*, 20210181.
- [4] X. Fang, S. Cai, M. Wang, Z. Chen, C. Lu, H. Yang, *Angew. Chem., Int. Ed.* **2021**, *60*, 7046.
- [5] J. Yao, Y. Liu, J. Wang, Q. Jiang, D. She, H. Guo, N. Sun, Z. Pang, C. Deng, W. Yang, S. Shen, *Biomaterials* **2019**, *195*, 51.
- [6] S. Li, R. Liu, X. Jiang, Y. Qiu, X. Song, G. Huang, N. Fu, L. Lin, J. Song, X. Chen, H. Yang, *ACS Nano* **2019**, *13*, 2103.
- [7] Z. Yang, Y. Luo, Y. Hu, K. Liang, G. He, Q. Chen, Q. Wang, H. Chen, *Adv. Funct. Mater.* **2020**, *31*, 2007991.
- [8] J. J. Lin, Y. Lin, T. Z. Zhao, C. K. Zhang, T. Zhang, X. L. Chen, J. Q. Ding, T. Chang, Z. Zhang, C. Sun, D. D. Zhao, J. L. Zhu, Z. Y. Li, J. L. Li, *Theranostics* **2017**, *7*, 2015.
- [9] H. F. Zhou, H. Yan, Y. Hu, L. E. Springer, X. Yang, S. A. Wickline, D. Pan, G. M. Lanza, C. T. Pham, *ACS Nano* **2014**, *8*, 7305.
- [10] S. Yao, Y. Wang, J. Chi, Y. Yu, Y. Zhao, Y. Luo, Y. Wang, *Adv. Sci.* **2022**, *9*, 2103449.
- [11] A. W. Carpenter, M. H. Schoenfish, *Chem. Soc. Rev.* **2012**, *41*, 3742.
- [12] Z. Luo, Y. Zhou, T. Yang, Y. Gao, P. Kumar, R. Chandrawati, *Small* **2022**, *18*, 2105762.
- [13] a) Z. Yang, Y. Yang, L. Zhang, K. Xiong, X. Li, F. Zhang, J. Wang, X. Zhao, N. Huang, *Biomaterials* **2018**, *178*, 1; b) H. Wu, Q. He, L. Li, L. Li, Z. Zhou, N. Chen, M. Yang, Q. Luo, B. Zhang, R. Luo, L. Yang, Y. Wang, *Chem. Eng. J.* **2022**, *427*, 130932.
- [14] Z. Du, X. Zhang, Z. Guo, J. Xie, X. Dong, S. Zhu, J. Du, Z. Gu, Y. Zhao, *Adv. Mater.* **2018**, *30*, 1804046.
- [15] Y. Ding, C. Du, J. Qian, C. M. Dong, *Nano Lett.* **2019**, *19*, 4362.
- [16] Z. Xue, M. Jiang, H. Liu, S. Zeng, J. Hao, *Biomaterials* **2020**, *263*, 120384.
- [17] M. Wang, Z. Hou, S. Liu, S. Liang, B. Ding, Y. Zhao, M. Chang, G. Han, A. A. A. Kheraif, J. Lin, *Small* **2021**, *17*, 2005728.
- [18] B. Xu, Y. Cui, W. Wang, S. Li, C. Lyu, S. Wang, W. Bao, H. Wang, M. Qin, Z. Liu, W. Wei, H. Liu, *Adv. Mater.* **2020**, *32*, 2003563.
- [19] B. Liu, S. Liang, Z. Wang, Q. Sun, F. He, S. Gai, P. Yang, Z. Cheng, J. Lin, *Adv. Mater.* **2021**, *33*, 2101223.
- [20] J. Mu, L. He, W. Fan, W. Tang, Z. Wang, C. Jiang, D. Zhang, Y. Liu, H. Deng, J. Zou, O. Jacobson, J. Qu, P. Huang, X. Chen, *Small* **2020**, *16*, 2004016.
- [21] a) Q. Zheng, B. Shi, F. Fan, X. Wang, L. Yan, W. Yuan, S. Wang, H. Liu, Z. Li, Z. L. Wang, *Adv. Mater.* **2014**, *26*, 5851; b) G.-T. Hwang, Y. Kim, J.-H. Lee, S. Oh, C. K. Jeong, D. Y. Park, J. Ryu, H. Kwon, S.-G. Lee, B. Joung, D. Kim, K. J. Lee, *Energy Environ. Sci.* **2015**, *8*, 2677; c) C. Dagdeviren, B. D. Yang, Y. Su, P. L. Tran, P. Joe, E. Anderson, J. Xia, V. Doraiswamy, B. Dehdashti, X. Feng, B. Lu, R. Poston, Z. Khalpey, R. Ghaffari, Y. Huang, M. J. Slepian, J. A. Rogers, *Proc. Natl. Acad. Sci. USA* **2014**, *111*, 1927; d) H. Ouyang, Z. Liu, N. Li, B. Shi, Y. Zou, F. Xie, Y. Ma, Z. Li, H. Li, Q. Zheng, X. Qu, Y. Fan, Z. L. Wang, H. Zhang, Z. Li, *Nat. Commun.* **2019**, *10*, 1821.
- [22] D. B. L. Teh, A. Bansal, C. Chai, T. B. Toh, R. A. J. Tucker, G. G. L. Gammad, Y. Yeo, Z. Lei, X. Zheng, F. Yang, J. S. Ho, N. Boleam, B. C. Wu, M. K. Gnanasammandhan, L. Hooi, G. S. Dawe, C. Libedinsky, W. Y. Ong, B. Halliwell, E. K. Chow, K. L. Lim, Y. Zhang, B. K. Kennedy, *Adv. Mater.* **2020**, *32*, 2001459.
- [23] a) F.-R. Fan, Z.-Q. Tian, Z. L. Wang, *Nano Energy* **2012**, *1*, 328; b) Y. Yang, N. Sun, Z. Wen, P. Cheng, H. Zheng, H. Shao, Y. Xia, C. Chen, H. Lan, X. Xie, C. Zhou, J. Zhong, X. Sun, S. T. Lee, *ACS Nano* **2018**, *12*, 2027; c) Y. Wu, Y. Luo, J. Qu, W. A. Daoud, T. Qi, *Nano Energy* **2019**, *64*, 103948.
- [24] a) X. Zhao, Z. Wang, Z. Liu, S. Yao, J. Zhang, Z. Zhang, T. Huang, L. Zheng, Z. L. Wang, L. Li, *Nano Energy* **2022**, *96*, 107067; b) Z. Wang, Z. Liu, G. Zhao, Z. Zhang, X. Zhao, X. Wan, Y. Zhang, Z. L. Wang, L. Li, *ACS Nano* **2022**, *16*, 1661.
- [25] a) Z. Liu, X. Liang, H. Liu, Z. Wang, T. Jiang, Y. Cheng, M. Wu, D. Xiang, Z. Li, Z. L. Wang, L. Li, *ACS Nano* **2020**, *14*, 15458; b) Z. Liu, J. Nie, B. Miao, J. Li, Y. Cui, S. Wang, X. Zhang, G. Zhao, Y. Deng, Y. Wu, Z. Li, L. Li, Z. L. Wang, *Adv. Mater.* **2019**, *31*, 1807795.
- [26] W. Guo, X. Zhang, X. Yu, S. Wang, J. Qiu, W. Tang, L. Li, H. Liu, Z. L. Wang, *ACS Nano* **2016**, *10*, 5086.
- [27] S. Du, N. Zhou, G. Xie, Y. Chen, H. Suo, J. Xu, J. Tao, L. Zhang, J. Zhu, *Nano Energy* **2021**, *85*, 106004.
- [28] H. Zou, Y. Zhang, L. Guo, P. Wang, X. He, G. Dai, H. Zheng, C. Chen, A. C. Wang, C. Xu, Z. L. Wang, *Nat. Commun.* **2019**, *10*, 1427.
- [29] J. U. Kim, H. Park, J. Ok, J. Lee, W. Jung, J. Kim, J. Kim, S. Kim, Y. H. Kim, M. Suh, T. I. Kim, *ACS Appl. Mater. Interfaces* **2022**, *14*, 15035.